Materials Characterization 147 (2019) 215–222

Contents lists available at ScienceDirect

Materials Characterization

journal homepage: www.elsevier.com/locate/matchar

Direct observation of monoclinic domains in rhombohedral $EuAl_3(BO_3)_4$ skeletal microcrystals

A.A. Mazilkin[a,b,*], O.G. Rybchenko[a], T.N. Fursova[a], S.Z. Shmurak[a], V.V. Kedrov[a]

[a] Institute of Solid State Physics, Russian Academy of Sciences, 142432 Chernogolovka, Russia
[b] Karlsruhe Institute of Technology (KIT), Institute of Nanotechnology, 76344 Eggenstein-Leopoldshafen, Germany

ARTICLE INFO

Keywords:
Infrared spectroscopy
Transmission electron microscopy
Europium aluminum borate
Polytypes
Cathodoluminance

ABSTRACT

The structural and spectroscopic features of the $EuAl_3(BO_3)_4$ individual skeletal microcrystals synthesized by a melt solution method have been studied. Their infrared spectra taken from the as-grown microcrystal surfaces mainly contain the lines of the rhombohedral modification of $EuAl_3(BO_3)_4$ and additional peaks of its monoclinic modification. TEM and X-ray diffraction studies confirm that these additional peaks in the IR spectra belong to the monoclinic *C2/c* polytype of the $EuAl_3(BO_3)_4$ compound. We are the first to demonstrate the presence of coherent monoclinic domains in rhombohedral $EuAl_3(BO_3)_4$ crystals by TEM. Cathodoluminance spectroscopy shows that the microcrystals generate strong emission lines in the range 580–630 nm, and their intensities are strongly influenced by the crystal orientation.

1. Introduction

In recent years, much attention has been paid to the study of rare earth aluminum borates $RM_3(BO_3)_4$ (R = rare earth atom, M = Al, Cr, Fe, Ga). They can be used in many applications, such as nonlinear optics, quantum electronics and laser technology [1,2], detectors and transformers of the ionizing radiation [3], and promising scintillators [4–7]. The radiation and chemical resistance of the aluminum borates, their thermal stability, and high thermal conductivity are important for practical applications [8]. The europium aluminum borate $EuAl_3(BO_3)_4$ is a phosphor with high color rendition in the red spectral range [9] and can be used as a promising material for LEDs [8,10].

Three crystal structures are known for the europium aluminum borate. These are a rhombohedral structure with space group *R32* (huntite structure) and two monoclinic structures, *C2/c* and *C2* (see Table 1). The rhombohedral phase was found to exist at lower temperatures than those of the monoclinic modifications of $EuAl_3(BO_3)_4$ [11–13].

The crystal structure of the $EuAl_3(BO_3)_4$ rhombohedral phase is shown in Fig. 1. Its main elements are EuO_6 trigonal prisms; AlO_6 octahedra; and two types of planar BO_3 groups, i.e. equilateral triangles with symmetry D_3 and isosceles triangles with symmetry C_2 [14]. These structural elements form two types of alternating compositional layers (Fig. 1b). Pairs of AlO_6 octahedra form the layer of the first type. The layer of the second type is composed of trigonal RO_6 prisms and AlO_6 octahedra. These structural elements in both layers are connected to each other by BO_3 triangles.

The three well-known crystalline structures of $EuAl_3(BO_3)_4$ form a family of polytypes. Each of them contains the aforementioned compositional layers in different stacking sequences (Belokoneva et al. [15]). Based on the stacking sequences, we have derived the following orientation relationships (OR) for these structures:

$$[0001]_{R32} \| [\bar{1}01]_{C2/c} \| [\bar{2}01]_{C2}$$
$$[\bar{1}010]_{R32} \| [\bar{2}01]_{C2/c} \| [\bar{5}02]_{C2}$$
$$[\bar{1}\bar{2}10]_{R32} \| [010]_{C2/c} \| [010]_{C2} \quad (1)$$

Aluminum borate crystals are usually prepared from a melt solution using various fluxes, such as $K_2Mo_3O_{10}$ or a mixture of PbO and PbF_2. Then, the synthesized crystals contain Mo and Pb [16] impurities, which negatively affect their optical properties and limit their applicability [5]. We used a new melt solution technique and took precursors free of molybdenum and lead as a flux [9]. As a result, we were able to form aluminum borate crystals without undesired impurities.

In [17], the individual microcrystals synthesized by this method and having different morphologies were investigated. There were crystals with full faces and those with a symmetrical pyramidal cavity on the upper face, so-called skeletal crystals. The spectral and structural characteristics of the crystals of both types were shown to coincide. According to Fourier transform infrared (FTIR) spectrometry, the

* Corresponding author at: Institute of Solid State Physics, Russian Academy of Sciences, 142432 Chernogolovka, Russia.
E-mail address: mazilkin@issp.ac.ru (A.A. Mazilkin).

https://doi.org/10.1016/j.matchar.2018.11.005
Received 4 August 2018; Received in revised form 15 October 2018; Accepted 3 November 2018
Available online 06 November 2018
1044-5803/

Table 1
Lattice parameters of $EuAl_3(BO_3)_4$ phases.

Crystal structure (space group)	Unit cell parameters	Ref.
R32 (155)	a = 0.9312 nm, c = 0.7275 nm	[11]
C2/c (15)	a = 0.722 nm, b = 0.9327 nm, c = 1.1074 nm, β = 103.17°	[12]
C2 (5)	a = 0.723 nm, b = 0.9322 nm, c = 1.6211 nm, β = 90.72°	[13]

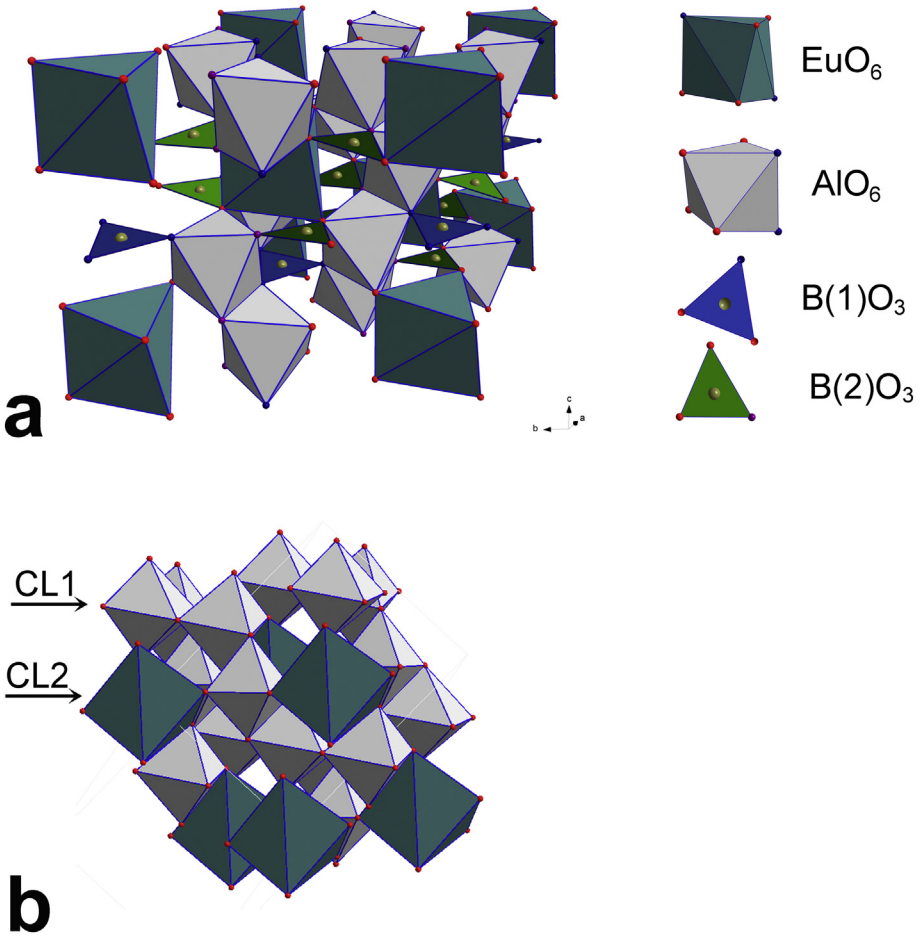

Fig. 1. (a) Crystal structure of $RAl_3(BO_3)_4$ with *R32* space group. Constituent polyhedra are shown at the right side. $B(1)O_3$ group is an equilateral triangle with symmetry D_3; $B(2)O_3$ group is an isosceles triangle with symmetry C_2. (b) Sequence of the compositional layers, CL1 and CL2, for *R32* crystal structure.

microcrystals had a rhombohedral structure and contained domains of another $EuAl_3(BO_3)_4$ polytype modification regardless of their morphology. Structural features in the form of a fringe contrast were observed by transmission electron microscopy (TEM), which can also indicate the presence of another phase in the rhombohedral matrix. Such bands were observed in aluminum borates of a complex composition [18,19]: these bands were supposed to be interchanging layers of rhombohedral and monoclinic phases.

The purpose of this work is to study of individual $EuAl_3(BO_3)_4$ skeletal microcrystals. The coexistence of two crystal phases is revealed by high-resolution TEM (HRTEM), X-ray diffraction (XRD), FTIR spectroscopy, and cathodoluminance (CL) spectroscopy.

2. Experimental

The microcrystals were prepared by the method described in [9]. IR reflection spectra were measured on Vertex 80v Fourier IR spectrometer with a resolution of 2 cm^{-1}. Reflection spectra were recorded from the as-grown microcrystal surfaces. The sizes of the detected area were set by means of the knife-edge aperture of a microscope. The reflection spectrum of an aluminum mirror was used as a reference. The resulting spectrum was obtained by division of the spectrum of a sample by the mirror spectrum. CL spectra were measured on a JSM 6490 scanning electron microscope equipped by a Gatan MonoCL3 CR system. The measurements were made at 10 keV, the electron beam current was about 0.1 nA, and the spectral resolution was about 0.5 nm.

The microstructure of the samples was studied by TEM on JEM-100CX microscope. TITAN 80–300 aberration corrected transmission electron microscope was used for HRTEM investigations. TEM samples were prepared by means of a focused ion beam on a VERSA 3D dual beam machine. Electron diffraction patterns were simulated using the JEMS software package [20].

Single-crystal XRD was performed on Gemini-R diffractometer (Oxford Diffraction, MoK_α radiation, graphite monochromator, ω-scanning). The processing of experimental data, including empirical correction for the absorption of the measured intensities and the calculation of the unit cell parameters, was performed with the CrysAlisPro software.

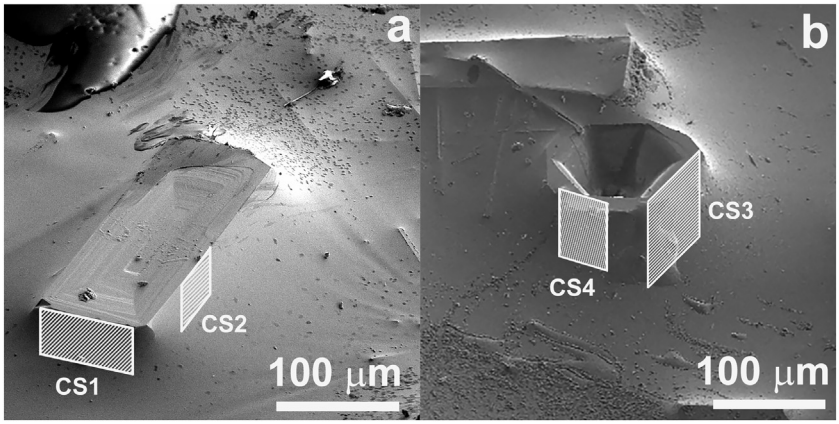

Fig. 2. $EuAl_3(BO_3)_4$ microcrystals: with (a) prismatic and (b) basal orientation of the as-grown face. Hatched rectangles indicate the position of cross sections.

3. Results and Discussion

According to the XRD data [17], the synthesized $EuAl_3(BO_3)_4$ microcrystals have the rhombohedral *R32* structure. They have two main orientations relative to the substrate: (i) a wide rectangular face emerges on the surface (Fig. 2a, prismatic orientation), and (ii) crystals are faceted in the form of hexagonal prisms, the basal plane of which is parallel to the surface (Fig. 2b, basal orientation).

3.1. FTIR Spectroscopy

The IR reflection spectra of $EuAl_3(BO_3)_4$ microcrystals were recorded in the range 600–1600 cm^{-1}, which is typical for internal B—O oscillations. The B—O bonds in the BO_3 groups of $EuAl_3(BO_3)_4$ lattice are stronger than the bonding forces of these groups with a cation sublattice. Therefore, the internal vibrations of BO_3 ions can be distinguished by analyzing vibrational spectra.

In the IR spectra of the huntite-type $RM_3(BO_3)_4$ compounds, the following vibration modes of the BO_3 groups can observed according to factor-group analysis [21]: one band of symmetric valence vibrations ν_1 (E); three bands of symmetric deformation vibrations ν_2 ($2A_2$ + E); and four bands of asymmetric valence and deformation vibrations, ν_3 and ν_4 (A_2 + 3E), respectively.

Fig. 3 shows the IR reflection spectra of $EuAl_3(BO_3)_4$ microcrystals from the as-grown faces of two orientations, namely, the basal (*FN* = $[0001]_{R32}$, Fig. 3a) and prismatic ones (*FN* = $<1210>_{R32}$, Fig. 3b). In the first case, the reflection light has **E⊥c** polarization, where **E** and **c** are the electric field and **c**-axis directions, respectively. The light is nonpolarized for the prismatic face. It means that the reflection spectra from almost all basal orientations are a combination of E and A_2 vibrational modes and resemble the absorption spectra of randomly oriented crystals.

The inset in Fig. 3a schematically shows the as-grown surface of a skeletal microcrystal of the basal orientation. The microcrystal has a height of 70 μm and the cavity depth is 36 μm. The IR reflection spectra from the basal plane was measured from the flat surface (area 1); the surface of the microcrystal cavity (area 2); and the entire crystal surface, including the flat region and the cavity (area 3). The identity of these spectra indicates that the structure of the microcrystal does not change through the entire depth of the crystal. The lower intensity of the reflection spectra from areas 2 and 3 is due to the light scattering on the stepped relief of the cavity surface. Since the cavity depth in a microcrystal with prismatic orientation is insignificant, the reflection spectrum was measured from the entire microcrystal surface (Fig. 3b).

A comparison of our data with the reflection spectra of isostructural compounds [22–24] gives the following results:

The most intense wide reflection bands in the frequency range

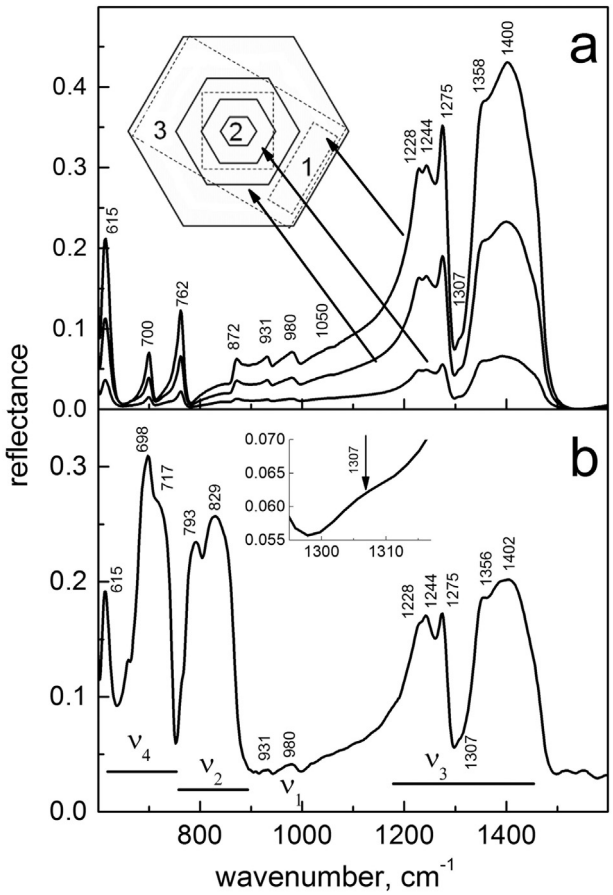

Fig. 3. FTIR reflection spectra of the as-grown faces of $EuAl_3(BO_3)_4$ microcrystals: (a) basal orientation *FN* = $[0001]_{R32}$, and (b) prismatic orientation. Insert in (a) shows the areas where three spectra were collected.

~1200–1450 cm^{-1}correspond to the asymmetric ν_3 valence vibrations. The bands in the range of 600–840 cm^{-1} are deformation vibrations ν_4, and ν_2 [25]. The weak band at ~980 cm^{-1} corresponds to the symmetric ν_1 valence vibration [21,26]. The two intense bands at ~1200 and ~1400 cm^{-1} within the stretching vibrations range ν_3 were attributed to the vibrational modes of two different BO_3 groups of the huntite structure having D_3 and C_2 local symmetry, respectively [22,27,28]. Both bands have a distinct fine structure: 1228, 1244 and 1275 cm^{-1} for BO_3 group with symmetry D_3, and 1358 and 1400 cm^{-1} for that with symmetry C_2. The doublet structure of the high-energy band at 1400 cm^{-1} is similar to that observed in the reflection spectrum

of $TbFe_3(BO_3)_4$ in the **E⊥c** polarization, which is a consequence of its splitting due to the low local symmetry of the BO_3 triangle (C_2) [22]. The observed fine band structure at 1200 cm^{-1}, which is related to the vibrations of BO_3 groups with local symmetry D_3, can be caused by the Fermi resonance between the overtone of deformation vibration ν_4 and asymmetric valence vibration ν_3. Both types of BO_3 groups were shown to participate in the formation of the lowest-energy ν_4 vibration mode [29]. This finding can cause the splitting of the band at 1200 cm^{-1} into three components, which was observed in our spectra.

An important conclusion that can be derived from an analysis of Fig. 3 is that the number of lines in these spectra is greater than that allowed by factor-group analysis. Additional weak lines at 931, 1050 and 1307 cm^{-1} are observed, as in the IR absorption spectra of rhombohedral $EuAl_3(BO_3)_4$ and $YAl_3(BO_3)_4$ macrocrystals several millimeters in size [26]. The authors of [26] suppose that these additional absorption lines are associated with the presence of monoclinic domains in the main *R32* phase. In particular, the weak band at 1310 cm^{-1} is characteristic of the IR spectra of rare-earth borates with space group *C2/c*. The band at 872 cm^{-1} in the reflection spectrum from the microcrystal basal plane (Fig. 3a) has not been observed earlier in the absorption spectrum of $EuAl_3(BO_3)_4$. This line was observed in the reflection spectrum of polarized light from the *R32* $YbAl_3(BO_3)_4$ compound and its origin was not discussed [24]. In general, the presence of additional alien bands is often observed in the IR spectra of rare-earth borates with a huntite structure [21,26,30,31].

Thus, the analysis of the IR reflection spectra permits us to assume the presence of domains of the monoclinic phase in rhombohedral $EuAl_3(BO_3)_4$ microcrystals. To the best of our knowledge, the microstructures of $EuAl_3(BO_3)_4$ crystals and other rear earth borates have not been directly observed. The choice between two monoclinic modifications of europium aluminum borate is still an open question.

3.2. TEM Studies

Several lift-out cross section (CS) lamellas from the synthesized aluminum borate crystals were prepared for TEM studies. The position of the CSs is shown in Fig. 2a and b. The images of the microstructure taken from four CSs and the corresponding electron diffraction patterns (DP) are given in Fig. 4. A fringe contrast is seen to be a distinctive feature of the microstructure in all four CSs: a system of parallel bands going through the entire sample at a certain angle to its surface. Such a contrast can correspond to the presumed monoclinic domains in the rhombohedral matrix of $EuAl_3(BO_3)_4$ microcrystal. The distance between the bands is different in various CSs of the microcrystal. They are least densely arranged in CS_1 and the average interband distance is 250 nm. For CS_3 and CS_2/CS_4 this distance is ~60 and ~85 nm, respectively.

The crystal structure of the domains is revealed from electron DPs. The simulated DPs are calculated using the JEMS software package based on the crystallographic data in Table 1. For an analysis of experimental DPs, combined stereographic projections are constructed for the rhombohedral and monoclinic crystals according to ORs (see Fig. 5).

The plane perpendicular to the long axis of the microcrystal (CS_1 in Fig. 2a) is the basal plane of the rhombohedral lattice with the normal direction indices $FN = [0001]_{R32}$, as follows from the DP in Fig. 4a. According to the OR, this plane is conjugated to the plane with $FN = [10\bar{1}]_{C2/c}$ in the *C2/2* lattice and to the plane with $FN = [20\bar{1}]_{C2}$ in the *C2* lattice. The DPs calculated for these three planes coincide with each other and we cannot conclude if more than one phase is present.

The plane parallel to CS_2 has normal $FN = [1010]_{R32}$ (Fig. 4b). The additional weak reflections, which center the rectangular network from the rhombohedral phase, correspond to the *C2/2* monoclinic phase with the normal to the sample plane, as is seen from Fig. 5a. The DPs from the planes in both monoclinic phases, which are conjugated to the planes $FN = [1100]_{R32}$ and $[0110]_{R32}$ of the rhombohedral lattice, coincide and do not contain additional reflections. These are planes with $FN = [2\bar{3}1]_{C2/c}$ and $[231]_{C2/c}$ of the *C2/c* phase. None of the conjugated planes of *C2* phase ($[502]_{C2}$, $[592]_{C2}$, and) contain additional spots in accordance to Fig. 5b.

The diffraction from CS_3 of the prismatic crystal (Fig. 4c) corresponds to the plane with $FN = <1210>_{R32}$ in the rhombohedral lattice. The conjugated planes with $FN = [211]_{C2/c}$, $[010]_{C2/c}$ and $[21\bar{1}]_{C2/c}$ in *C2/c* give coincident DPs with no additional reflections, as well as with $FN = [532]_{C2}$ and $[\bar{5}32]_{C2}$. If the *C2* phase was present in the sample, the $[010]_{C2}$ section conjugated with $FN = [1210]_{R32}$ would contain additional spots (see Fig. 5b). However, this is not the case.

The DP from CS_4 also shows no extra spots and can be interpreted either as a plane with the normal $FN = [1100]_{R32}$ or as a conjugated plane with $FN = [231]_{C2/c}$ and $[\bar{2}31]_{C2/c}$, as well as, $\langle 592\rangle_{C2}$ and $\langle 532\rangle_{C2}$ in the corresponding monoclinic modifications of $EuAl_3(BO_3)_4$. All simulated DPs from monoclinic phases contain no additional spots, as observed in the experimental pattern.

Thus, based on an analysis of the DPs, the $EuAl_3(BO_3)_4$ microcrystals with a rhombohedral lattice are found to contain monoclinic *C2/c* phase domains.

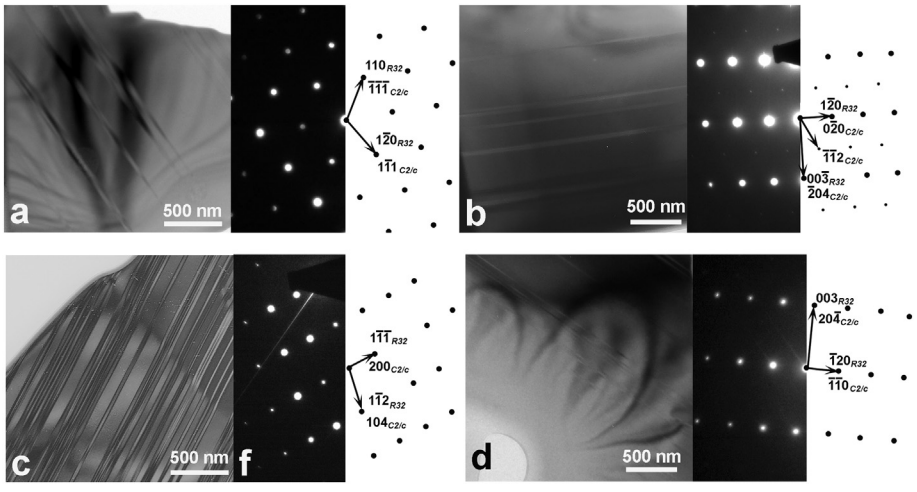

Fig. 4. Microstructure of $EuAl_3(BO_3)_4$ microcrystals in four different CSs with corresponding DP: (a), (b) $FN = [1010]_{R32}$, (c) $FN = [1210]_{R32}$, and (d) $FN = [1100]_{R32}$. DPs are indexed using both the rhombohedral (*R32*) and monoclinic (*C2/c*) lattices. The positions of CSs are schematically shown in Fig. 2.

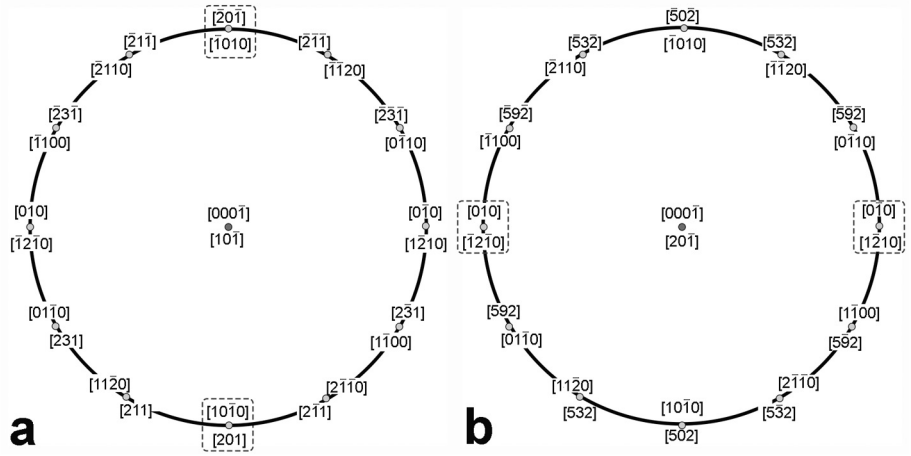

Fig. 5. Combined stereographic projections of an $EuAl_3(BO_3)_4$ crystal of rhombohedral *R32* and (a) *C2/c*, and (b) *C2* monoclinic lattices. Directions in rhombohedral lattice are shown by four indexes. The poles in dashed boxes show additional reflections in DPs.

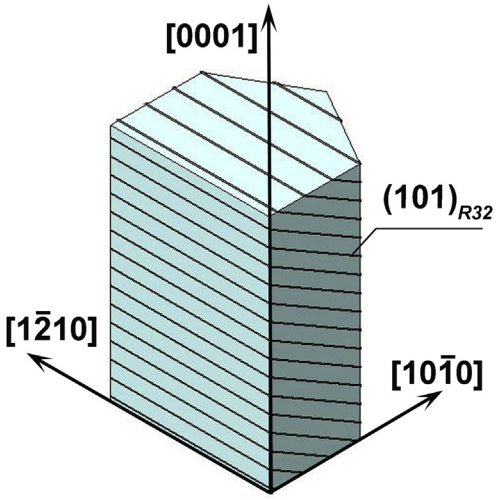

Fig. 6. Schematic view of the $EuAl_3(BO_3)_4$ microcrystal habit. The crystal is faceted by six prismatic ($FN = <1210>_{R32}$) and two basal ($FN = [0001]_{R32}$) planes. Lines on the faces denote the emergence of the monoclinic domain boundaries. The crystal is sectioned to show the face with $FN = <1010>_{R32}$. Domain boundaries are parallel to $(101)_{R32}$ plane. For simplicity, domains boundaries are drawn at equal distances. The distances between the traces on different faces are seen to be different.

The habit planes of the microcrystals can be determined using the electron diffraction data. The direction along which a crystal is elongated is the normal to the basal plane [0001], and the prismatic faces have a normal along the $\langle 1210\rangle_{R32}$ directions (Fig. 6). This habit corresponds to that usually observed for rare-earth aluminum borate macrocrystals [32].

Based on trace analysis of the bands (Fig. 4), we found that they lie in the $(101)_{R32} \parallel (001)_{C2/c}$ plane, i.e., in the conjugation plane of the compositional layers that are common for the *R32* and *C2/c* lattices. The scheme in Fig. 6 also shows that, for equidistant arrangement of domains in the $(101)_{R32}$ plane, the distance between their traces on different crystal faces is different. This finding can explain our observation of different spacing between the monoclinic domains in the microcrystals (see Fig. 4).

3.3. XRD Studies

The presence of the monoclinic phase was also confirmed by single-crystal XRD studies. For this purpose, several crystals of the prismatic and basal orientations were carefully detached from the substrate. All of them were of good quality, i.e. transparent and without twins. The parameters of the main phase, which is responsible for most observed XRD peaks, coincide with the data reported for $EuAl_3(BO_3)_4$: the space group is *R32*, $a = 0.931–0.932$ nm, and $c = 0.727–0.728$ nm.

In addition to the reflections from the main phase, weak reflections are observed (Fig. 7). The DP in Fig. 7a shows the section of the

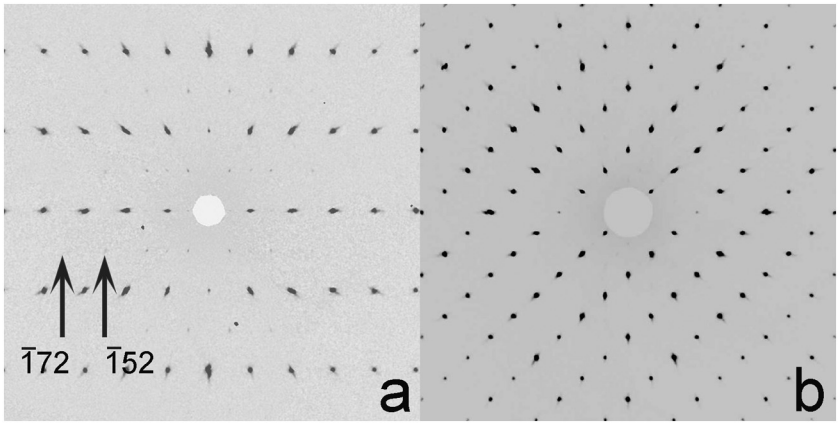

Fig. 7. Sections of single crystal XRD data (a) $FN = [1010]_{R32}$ and (b) one of the plane with $FN = <1210>_{R32}$. Two weak reflections are shown in (a) with a relative intensity $I_{\bar{1}52}/I_{\bar{1}72} \approx 180/1$.

reciprocal space parallel to the $(300)_{R32}$ plane of the rhombohedral lattice. The analysis as in the case of the diffraction pattern of CS_2 shows that the additional spots belong to the $(202)_{C2/c}$ plane of the monoclinic phase with space group *C2/c*.

As can be seen in Fig. 7, the additional reflections have low intensities and are only observed in the central part of the diffraction pattern. This is due to a significant decrease in the scattering amplitude as the diffraction angle increases. The calculated intensity ratio for the reflections $\left(\bar{1}52\right)$ and $\left(\bar{1}72\right)$ is $I_{\bar{1}52}/I_{\bar{1}72} \approx 180/1$. It should be taken into account that the main reflections in the DP are a superposition of reflections from two phases, i.e., rhombohedral and monoclinic, because of the coherence of their conjugation.

XRD analysis shows that there are no additional reflections from the *C2* phase in all $<1\bar{2}10>_{R32}$ planes of the microcrystals (Fig. 7b). Therefore, it confirms that only monoclinic *C2/c* phase domains are present in the microcrystals. The fraction of this phase could not be adequately estimated due to the very low intensity of superstructural reflections. It is necessary to note that the structural analysis itself was not the subject of our research; therefore, we did not perform structure refinement and did not calculate the R-factor.

3.4. HRTEM Studies

We carried out an HRTEM study to demonstrate that the areas of dark contrast in Fig. 4 correspond to monoclinic-phase domains. Some HRTEM images from part of the sample containing a fringe contrast are shown in Fig. 9. The areas that differ in contrast with respect to the surrounded material are visible in all three images. They have a width of 10–15 nm and completely coherent boundaries and no signs of defects such as twins or misfit dislocations are revealed. The fast Fourier transforms (FFTs) of the HRTEM images are also shown in Fig. 8. An analysis of FFTs is the same as for all diffraction patterns. Similarly to DPs in Fig. 4b, additional reflections appear in FFT pattern from area 2 of CS_2 ($FN = [1\bar{2}10]_{R32}$, Fig. 8b). There are no additional reflections from area 1 of the same sample. For the two remaining CSs, the FFT patterns from the main crystal and the monoclinic phase coincide and no additional reflections are expected to be observed in them. Thus, area 2 is concluded to be a *C2/c* monoclinic domain in the rhombohedral crystal. Taking into account the coherence of the interphase boundary, the second-phase inclusions can be represented as regions with an alternating order of compositional layers. The possibility of coexistence of differently ordered borate polytypes and their coherence was pointed out in [15], where this phenomenon was attributed to the temperature gradient during crystallization.

Thus, using HRTEM investigations, we were the first to detect *C2/c* monoclinic domains inside the rhombohedral matrix of $EuAl_3(BO_3)_4$ skeletal microcrystals.

3.5. CL Spectroscopy

We carried out CL measurements of the synthesized microcrystals to find their spectral characteristics. The CL spectra of the as-grown microcrystal surfaces (prismatic and basal faces), and the lift-out samples with CS_1 ($FN = [0001]_{R32}$), CS_2 ($FN = [1\bar{2}10]_{R32}$), and CS_3 ($FN = [10\bar{1}0]_{R32}$) were compared.

Two pairs of bands are most intense in the CL spectra (Fig. 9). They correspond to the electron transitions in the Eu^{3+} ion with maxima at 591 and 596 nm ($^5D_0 \rightarrow {}^7F_1$ transition) and 613 and 618 nm ($^5D_0 \rightarrow {}^7F_2$ transition). The same bands were observed earlier in the photoluminescence spectra of full faced microcrystals and in the CL study of skeletal microcrystals [9,17]. The intensity ratio for the peaks at 613 and 618 nm (~2:1) is equal for both as-grown surfaces and three CSs. In contrast, the intensity ratio changes for the $^5D_0 \rightarrow {}^7F_1$ transition bands depending on the orientation of the sample plane. For CS_2 and CS_4 and the as-grown prismatic face ($FN = [1\bar{2}10]_{R32}$), the intensity ratio almost coincides and is ~1.3. For the basal plane (both as-grown surface and CS_1) this ratio is ~2.6. The coincidence of the CL spectra of the as-grown surfaces and CSs with the same crystallographic orientation confirms the following conclusion drawn from FTIR spectroscopy data: the microcrystals have a homogeneous structure.

The electron transitions between the $4f^n$ states in rare earth R^{3+} ions are optically active and determine the composition of the luminescence spectra [33,34]. These transitions are parity forbidden and can be partially allowed in the crystal field. The interaction energy of 4f electrons with the crystal field is much larger than the spectral line

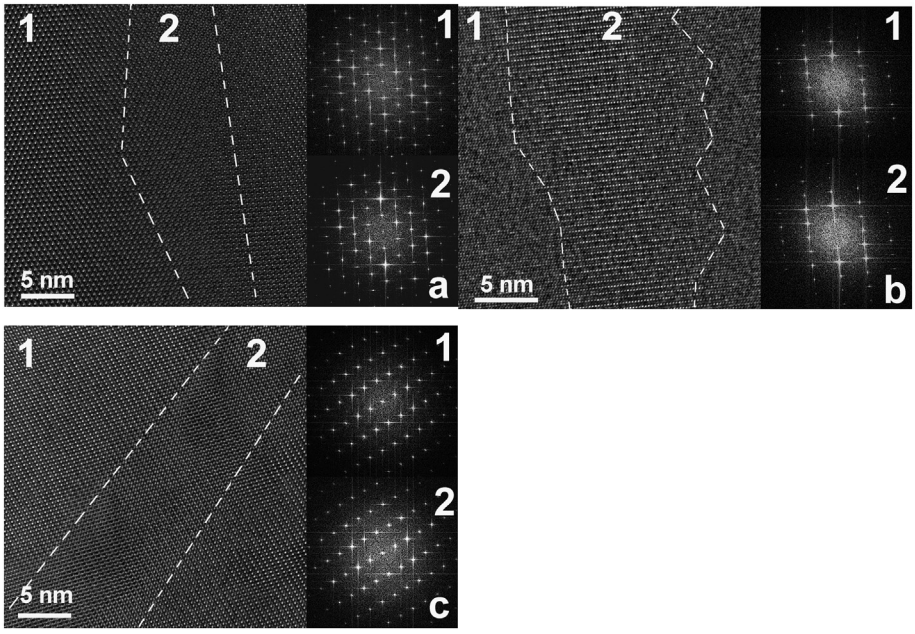

Fig. 8. HRTEM images and corresponding FFT patterns for the $EuAl_3(BO_3)_4$ lift-out samples with (a) $FN = [0001]_{R32}$, (b) $FN = [1\bar{2}10]_{R32}$, and (c) $FN = [10\bar{1}0]_{R32}$. The areas of rhombohedral matrix (1) and monoclinic domain (2) are denoted in the images.

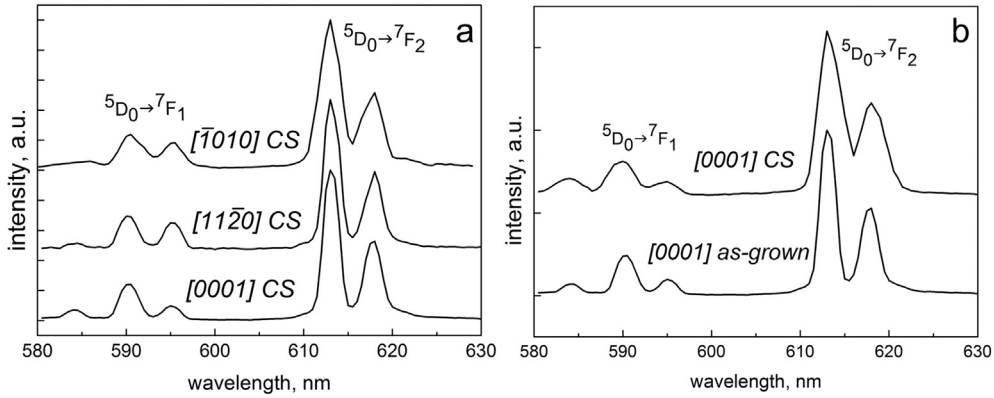

Fig. 9. (a) CL spectra of $EuAl_3(BO_3)_4$ microcrystals from different CSs; (b) comparison of CL spectra from CS and as-grown face for basal plane of rhombohedral crystal $FN = [0001]_{R32}$.

widths of the $4f^n$ transitions. Therefore, R^{3+} ions are very sensitive to the nearest environment. When their local symmetry changes, the spectral composition also changes. For example, the positions of the main peaks in the photoluminescence spectra of Eu^{3+} ions in the monoclinic α-phase and the orthorhombic β´-phase of $Eu_2(MoO_4)_3$ differ by ~1 nm [35–37].

TEM data show that the number of traces from monoclinic domains emerging to the crystal surface changes as a function of its orientation. It could lead to different contributions to a CL signal from different phases in a sample and, consequently, to changes in its spectral composition. Two types of spectral changes are possible: the appearance of new lines and a change in the relative lines intensity. Analyzing the spectra in Fig. 9, we should take into account the following two points. Because of a weak signal intensity, the CL spectra were recorded using wide spectrometer slits (0.5–1 mm), which leads to a substantial increase in the peak width (full width at half maximum is ~2.5–2.8 nm). Such broadened peaks did not allow us to recognize small changes in the positions of the CL maxima corresponding to the different crystallographic modifications of $EuAl_3(BO_3)_4$. Second, the assumption that the monoclinic phase can contribute differently to luminescence depending on the crystallographic orientation is only valid for the case when the collected signal is excited in the limited volume comparable with the monoclinic-domain size. The interaction volume for a CL signal is several microns, which means that the amount of the phase that contributes to the signal cannot depend on the sample orientation. The coincidence of the CL spectra of the as-grown faces and CSs with the same orientations confirms this conclusion.

Another possible explanation of the change in the spectral relative intensity is the orientation dependence of the CL spectra. Based on spectroscopic studies of the YPO_4(Nd) and $ZrSiO_4$ compounds, the authors of [38] showed that the relative intensities of certain luminescence bands are strongly influenced by the crystal orientation. Therefore, we can conclude that the change in the relative intensities of the 591 and 595 nm lines in Fig. 9 is most likely to be due to the orientation dependence of the CL spectra.

4. Conclusions

1. Using direct structural HRTEM studies, we were the first to show that the additional lines in the IR spectra of $EuAl_3(BO_3)_4$ microcrystals correspond to monoclinic domains of this phase.
2. Structural investigations confirmed that the domains have a *C2/c* crystal structure and are coherently conjugated to the rhombohedral lattice of the matrix along the $(101)_{R32}$ plane, where the stacking sequence of compositional layers changes in different polytypes structure;
3. An orientation dependence of the relative CL line intensities is revealed for $EuAl_3(BO_3)_4$ microcrystals.

Data Availability

The raw/processed data required to reproduce these findings cannot be shared at this time due to technical or time limitations. They can be shared on demand.

Acknowledgements

The work was supported by the Ministry of Education and Science of the Russian Federation (Agreement no. 14.B25.31.0018). This work was partly carried out with the support of the Karlsruhe Nano Micro Facility (KNMF, www.knmf.kit.edu), a Helmholtz Research Infrastructure at Karlsruhe Institute of Technology (KIT, www.kit.edu) and the scientific facilities of the Institute of Solid State Physics, Russian Academy of Sciences. The authors are grateful to Dr. Salavat Khasanov for his help in XRD measurements and discussion of the results.

References

[1] R. Arun Kumar, Borate crystals for nonlinear optical and laser applications: a review, J. Chem. 2013 (2013) 1–6, https://doi.org/10.1155/2013/154862.
[2] D. Xue, K. Betzler, H. Hesse, D. Lammers, Nonlinear optical properties of borate crystals, Solid State Commun. 114 (2000) 21–25, https://doi.org/10.1016/S0038-1098(99)00579-7.
[3] M. Ishii, Y. Kuwano, S. Asaba, T. Asai, M. Kawamura, N. Senguttuvan, T. Hayashi, M. Koboyashi, M. Nikl, S. Hosoya, K. Sakai, T. Adachi, T. Oku, H.M. Shimizu, Luminescence of doped lithium tetraborate single crystals and glass, Radiat. Meas. 38 (2004) 571–574, https://doi.org/10.1016/J.RADMEAS.2004.03.017.
[4] J.H. Huang, Y.J. Chen, X.H. Gong, Y.F. Lin, Z.D. Luo, Y.D. Huang, Growth, polarized spectral properties, and 1.5–1.6 μm laser operation of Er:Yb:Sr3Gd2(BO3)4 crystal, Appl. Phys. B Lasers Opt. 97 (2009) 431–437 mater https://doi.org/10.1007/s00340-009-3570-4.
[5] X. Yu, Y. Yue, J. Yao, Z. Hu, YAl3(BO3)4: crystal growth and characterization, J. Cryst. Growth 312 (2010) 3029–3033, https://doi.org/10.1016/j.jcrysgro.2010.07.005.
[6] G.E. Malashkevich, V.N. Sigaev, N.V. Golubev, E.K. Mamadzhanova, A.A. Sukhodola, A. Paleari, P.D. Sarkisov, A.N. Shimko, Spectroscopic properties of Sm-containing yttrium-aluminoborate glasses and analogous huntite-like polycrystals, Mater. Chem. Phys. 137 (2012) 48–54, https://doi.org/10.1016/j.matchemphys.2012.07.055.
[7] P.P. Pawar, S.R. Munishwar, S. Gautam, R.S. Gedam, Physical, thermal, structural and optical properties of Dy3+ doped lithium alumino-borate glasses for bright W-LED, J. Lumin. 183 (2017) 79–88, https://doi.org/10.1016/J.JLUMIN.2016.11.027.
[8] N.I. Leonyuk, Growth of new optical crystals from boron-containing fluxed melts, Crystallogr. Rep. 53 (2008) 511–518, https://doi.org/10.1134/S106377450803022X.
[9] S.Z. Shmurak, V.V. Kedrov, A.P. Kiselev, I.I. Zver'kova, Evolution of the spectral characteristics upon annealing of lithium borate glasses containing europium and aluminum, Phys. Solid State 55 (2013) 377–384, https://doi.org/10.1134/S1063783413020261.
[10] B.C. Jamalaiah, J.S. Kumar, A.M. Babu, L.R. Moorthy, Spectroscopic studies of Eu3+ ions in LBTAF glasses, J. Alloys Compd. 478 (2009) 63–67, https://doi.org/10.1016/j.jallcom.2008.12.013.
[11] A.D. Prokhorov, E.E. Zubov, A.A. Prokhorov, L.F. Chernush, R. Minyakaev, V.P. Dyakonov, H. Szymczak, EPR spectra of Cr 3+ ion in the Van Vleck

paramagnet EuAl 3 (BO3)4, Phys. Status Solidi 250 (2013) 1331–1338, https://doi.org/10.1002/pssb.201248571.
[12] E.L. Belokoneva, M.A. Simonov, A.V. Pashkova, T.I. Timchenko, N.V. Belov, Crystal structure of high-temperature monoclinal modification of Nd, Al-bortae, NdAl3(BO3)4, Dokl. Akad. Nauk SSSR 255 (1980) 854–858.
[13] P.A. Plachinda, E.L. Belokoneva, High temperature synthesis and crystal structure of new representatives of the huntite family, Cryst. Res. Technol. 43 (2008) 157–165, https://doi.org/10.1002/crat.200711071.
[14] E.L. Belokoneva, A.V. Azizov, N.I. Leonyuk, M.A. Simonov, N.V. Belov, Crystal structure of Yal3[BO3]4, J. Struct. Chem. 22 (1981) 476–478, https://doi.org/10.1007/BF00747537.
[15] E.L. Belokoneva, T.I. Timchenko, Polytypic relationships in structures of borates with the general formula $RAl_3(BO_3)_4$ (R = Y, Nd, Gd), Kristallographiya 28 (1983) 1118–1132.
[16] N.I. Leonyuk, L.I. Leonyuk, Growth and characterization of RM3(BO3)4 crystals, Prog. Cryst. Growth Charact. Mater. 31 (1995) 179–278, https://doi.org/10.1016/0960-8974(96)83730-2.
[17] T.N. Fursova, S.Z. Shmurak, V.V. Kedrov, O.G. Rybchenko, E.B. Yakimov, A.A. Mazilkin, Spectral and structural investigations of EuAl3(BO3)4 microcrystals, Phys. Solid State 59 (2017).
[18] E.V. Koporulina, N.I. Leonyuk, A.V. Mokhov, O.V. Pilipenko, Crystal growth and characterization of the (Y, RE)Al3(BO3)4 solid solution (RE = Nd, Gd, Ho, Yb, Lu), J. Solid State Chem. 154 (2000), https://doi.org/10.1006/jssc.2000.8856.
[19] N.I. Leonyuk, E.V. Koporulina, J.Y. Wang, X.B. Hu, A.V. Mokhov, Neodymium and chromium segregation at high-temperature crystallization of (Nd,Y)Al3(BO3)4 and (Nd,Y)Ca4O(BO3)3 doped with Cr3+, J. Cryst. Growth 252 (2003) 174–179, https://doi.org/10.1016/S0022-0248(02)02437-5.
[20] P. Stadelmann, JEMS Software Package for Electron Microscopy, http://www.jems-saas.ch/.
[21] V.S. Kurazhkovskaya, E.Y. Borovikova, N.I. Leonyuk, E.V. Koporulina, E.L. Belokoneva, Infrared spectroscopy and the structure of polytypic modifications of RM3(BO3)4 borates (R - Nd, Gd, Y; M - Al, Ga, Cr, Fe), J. Struct. Chem. 49 (2008) 1035–1041, https://doi.org/10.1007/s10947-008-0175-4.
[22] M.I. Pashchenko, V.A. Bedarev, V.I. Kut'ko, L.N. Besmaternykh, V.L. Temerov, IR active vibrations of a TbFe3(BO3)4 crystal, Low Temp. Phys. 36 (2010) 638–641, https://doi.org/10.1063/1.3479413.
[23] K.N. Boldyrev, D.A. Erofeev, IR active phonons in single crystals RFe3(BO3)4 (R = Pr, Nd, and Sm), Opt. Spectrosc. 116 (2014) 872–877, https://doi.org/10.1134/S0030400X14060034.
[24] K.N. Boldyrev, B.N. Mavrin, M.N. Popova, L.N. Bezmaternykh, Spectroscopy of phonon and vibronic states of YbAl3(BO3)4 single crystal, Opt. Spectrosc. (2011), https://doi.org/10.1134/S0030400X11090049.
[25] E.A. Dobretsova, Complex Research of Rare-Earth Aluminum, Chrome and Gallium Borates with Huntite Structure, Institute of Spectroscopy, Russian Academy of Sciences, 2016, https://isan.troitsk.ru/static/docs/diss/Dobretsova-thesis.pdf , Accessed date: 30 September 2017.
[26] E.A. Dobretsova, E.Y. Borovikova, K.N. Boldyrev, V.S. Kurazhkovskaya, N.I. Leonyuk, IR spectroscopy of rare-earth aluminum borates RAl3(BO3)4 (R = Y, Pr-Yb), Opt. Spectrosc. 116 (2014) 77–83, https://doi.org/10.1134/S0030400X14010068.
[27] S.N. Sofronova, Y.V. Gerasimova, A.N. Vtyurin, I.A. Gudim, N.P. Shestakov, A.A. Ivanenko, Infrared absorption spectrum of HoFe3(BO3)4 crystal, Vib. Spectrosc. 72 (2014) 20–25, https://doi.org/10.1016/j.vibspec.2014.02.005.
[28] Y.V. Gerasimova, S.N. Sofronova, I.A. Gudim, A.S. Oreshonkov, A.N. Vtyurin, A.A. Ivanenko, Infrared absorption spectra of a Nd0.5Ho0.5Fe3(BO3)4 crystal, Phys. Solid State 58 (2016) 155–159, https://doi.org/10.1134/S106378341601011X.
[29] V.A. Chernyshev, A.E. Nikiforov, V.P. Petrov, A.V. Serdtsev, M.A. Kashchenko, S.A. Klimin, Structure and lattice dynamics of rare-earth ferroborate crystals: Ab initio calculation, Phys. Solid State 58 (2016) 1642–1650, https://doi.org/10.1134/S1063783416080096.
[30] E.Y. Borovikova, K.N. Boldyrev, S.M. Aksenov, E.A. Dobretsova, V.S. Kurazhkovskaya, N.I. Leonyuk, A.E. Savon, D.V. Deyneko, D.A. Ksenofontov, Crystal growth, structure, infrared spectroscopy, and luminescent properties of rare-earth gallium borates RGa3(BO3)4, R = Nd, Sm-Er, y, Opt. Mater. 49 (2015) 304–311, https://doi.org/10.1016/j.optmat.2015.09.021 (Amst).
[31] E.Y. Borovikova, E.A. Dobretsova, K.N. Boldyrev, V.S. Kurazhkovskaya, V.V. Maltsev, N.I. Leonyuk, Vibrational spectra and factor group analysis of rare-earth chromium borates, RCr3(BO3)4, with R = La-Ho, Vib. Spectrosc. 68 (2013) 82–90, https://doi.org/10.1016/j.vibspec.2013.05.004.
[32] N.I. Leonyuk, A.V. Pashkova, T.D. Semenova, Inorg. Mater. 11 (1975) 181 (in Russian).
[33] M.A. Elyashevich, Spectra of the Rare Earths, Atomic Energy Commission, Washington, DC, 1961.
[34] M.I. Gaiduk, V.F. Zolin, L.S. Gaigerova, Luminescence Spectra of Europium, Nauka, Moscow, 1974 (in Russian).
[35] A.P. Kiselev, S.Z. Shmurak, B.S. Red'kin, V.V. Sinitsyn, I.M. Shmyt'ko, E.A. Kudrenko, E.G. Ponyatovskiĭ, Evolution of the spectral response of amorphous europium molybdate under annealing, Phys. Solid State 48 (2006) 1544–1552, https://doi.org/10.1134/S1063783406080208.
[36] S.Z. Shmurak, A.P. Kiselev, N.V. Klassen, V.V. Sinitsyn, I.M. Shmyt'ko, B.S. Red'kin, S.S. Khasanov, Modifications of light emission spectra and atomic structure of europium molibdate bulk crystals caused by high pressure and heat treatment, IEEE Trans. Nucl. Sci. (2008) 1128–1132, https://doi.org/10.1109/TNS.2008.924049.
[37] S.Z. Shmurak, A.P. Kiselev, D.M. Kurmasheva, B.S. Red'kin, V.V. Sinitsyn, Effect of solid-phase amorphization on the spectral characteristics of europium-doped gadolinium molybdate, J. Exp. Theor. Phys. 110 (2010) 759–768, https://doi.org/10.1134/S1063776110050055.
[38] C. Lenz, D. Talla, K. Ruschel, R. Škoda, J. Götze, L. Nasdala, Factors affecting the Nd3+ (REE3+) luminescence of minerals, Mineral. Petrol. 107 (2013) 415–428, https://doi.org/10.1007/s00710-013-0286-2.